



# Refinement of the $\gamma$ phase with melt undercooling in a two-phase $\text{Co}_2\text{NiGa}$ magnetic shape memory alloy

J.Z. Li, J. Liu, M.X. Zhang, J.G. Li\*

School of Materials Science and Engineering, Shanghai Jiao Tong University, Shanghai 200240, PR China

## ARTICLE INFO

### Article history:

Received 14 January 2010

Accepted 20 January 2010

Available online 1 February 2010

### Keywords:

Co–Ni–Ga

Undercooling

Refinement

Magnetic shape memory alloy

## ABSTRACT

The effect of melt undercooling on the  $\gamma$  phase is investigated in a two-phase  $\text{Co}_2\text{NiGa}$  magnetic shape memory alloy by employing the method of glass fluxing combined with superheating cycling. A maximum bulk undercooling of 230 K is achieved. Microstructural evolution of the  $\text{Co}_2\text{NiGa}$  alloy is investigated by optical microscopy with respect to different degrees of undercooling. Over the whole range of undercooling, it is found that both the size and the volume fraction of the  $\gamma$  phase are drastically influenced by undercooling. Especially, when the undercooling is in the range of 190–230 K, the alloy has an obvious preferred orientation.

© 2010 Elsevier B.V. All rights reserved.

## 1. Introduction

As a new ferromagnetic shape memory alloy (FSMA), Co–Ni–Ga has recently attracted a great deal of interest. Compared with Ni–Mn–Ga alloys, which tend to be single-phase, Co–Ni–Ga alloys show relatively higher ductility due to the secondary-phase (fcc  $\gamma$ -phase) presence [1]. Additionally, Co–Ni–Ga alloys have relatively high Curie temperature ( $T_c$ ) [2]. As to potential application, a two-way shape memory effect was reported in single-crystalline Co–Ni–Ga alloys [3]. It has been widely recognized that the coarse matrix  $\beta$  phase (bcc structure) and the fine  $\gamma$  phase at grain boundaries are of typical microstructural features [1,4]. Since the morphology of the  $\gamma$  phase plays an important role in influencing alloy properties, to control the  $\gamma$  phase morphology is essential for the development of the new FSMA. Approaches of controlling the size, shape and distribution of the  $\gamma$  phase can be realized by tailoring the parameters in solidification or heat treatment. Since the solidified microstructure is crucial in determining the final morphology of the  $\gamma$  phase, controllable solidification, e.g. rapid undercooling solidification, is therefore utilized when the evolution of microstructure in Co–Ni–Ga alloys is probed into.

Rapid solidification of undercooled alloy melts is an attractive subject in both structural and functional material studies [5]. The structural evolution and phase selection of undercooled melts have been widely investigated in Ni–Cu alloys [6,7], superalloys (such as DD3 alloys) [8,9] and Fe–Ga alloys [10,11]. It is verified that

if the melts reach a certain undercooling, the alloys tend to possess a solidification texture and refined grains can be obtained. Besides, a metastable phase of  $\text{DO}_3$  responsible for large magnetostriction can be induced by a large degree of undercooling [12]. However, few detailed research is distinguished concerning the effect of undercooling on FSMA. Our previous work has pointed out that the martensitic transformation temperature ( $M_s$ ) and crystal structure can be changed in single-phase  $\text{Co}_{46}\text{Ni}_{27}\text{Ga}_{27}$  under different undercooling conditions [13]. In the current study, we focus on stoichiometric  $\text{Co}_2\text{NiGa}$  with two phases, especially dealing with the morphology and the size of  $\gamma$  phase at different degrees of melt undercooling.

## 2. Experimental

Polycrystalline ingots of  $\text{Co}_2\text{NiGa}$  alloys were prepared from Co (99.97% purity), Ni (99.96% purity) and Ga (99.99% purity) by arc-melting under an argon atmosphere. The ingots were melted four times and homogenized in a vacuum heat treatment furnace at 1273 K for 48 h in order to achieve composition homogenization. Samples with the mass in 1.5 g were cut from the ingots for the undercooling experiments which were performed in an apparatus (Fig. 1). Glass fluxing combined with superheating cycling was used to achieve a reasonable large undercooling. The  $\text{Na}_2\text{B}_4\text{O}_7$  glass was employed as the purifier to suppress nucleation, and high frequency induction heating under the protection of an argon atmosphere was conducted.

In the undercooling experiment, in order to obtain a large undercooling, the  $\text{Co}_2\text{NiGa}$  sample was superheated to 1773 K for 1.5 min and then subjected to superheating-cooling cycle for four times. The cooling curve of the melt was measured by an infrared pyrometer, which was calibrated with a standard PtRh<sub>30</sub>–PtRh<sub>6</sub> thermocouple, a relative accuracy of 5 K and a response time less than 1 ms.

Metallographic specimens were polished and etched with the solution consisting of 5 g  $\text{FeCl}_3$  + 25 ml  $\text{HCl}$  + 100 ml  $\text{H}_2\text{O}$ . Microstructure morphology was observed through a Neophot-1 optical microscope. Composition was determined by energy dispersion X-ray spectroscopy (EDS). The crystal structure was analyzed by X-ray diffraction analysis (D/max 2550 V XRD) with  $\text{Cu K}_\alpha$  radiation.

\* Corresponding author.

E-mail addresses: [junzhengli@sjtu.edu.cn](mailto:junzhengli@sjtu.edu.cn) (J.Z. Li), [lijg@sjtu.edu.cn](mailto:lijg@sjtu.edu.cn) (J.G. Li).

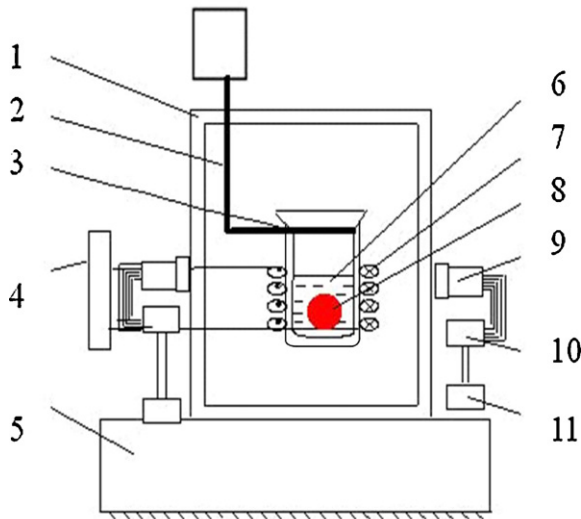


**Fig. 1.** Sketch of the apparatus for undercooling experiments. (1) Vacuum chamber; (2) up-down withdrawing system; (3) two-double silica crucible; (4) SIT high frequency power supply; (5) Bear frame; (6) fluxing glass; (7) induction coils; (8) sample; (9) infrared thermodetector; (10) signal processing unit; (11) grapher recording meter.

### 3. Results and discussion

The maximum undercooling for  $\text{Co}_2\text{NiGa}$  alloys reached 230 K. Fig. 2 shows a typical cooling curve of undercooled  $\text{Co}_2\text{NiGa}$  (the degree of undercooling,  $\Delta T = 230$  K) alloy melts. By the combination of glass purification and superheating cycling, possible nuclear particles were removed and passivated, thus purification was achieved in the melts. When the melt was cooled to the nucleation temperature ( $T_N$ ), the sample would abruptly nucleate and solidify due to any disturbance from the crystal surface. Because of the latent heat releasing from the solidified phase, the system temperature quickly rose to recalescence temperature ( $T_R$ ). After that, the specimen started a slow cooling down till room temperature.

The EDS analysis of rapidly solidified samples with different melt undercooling of 0–230 K confirms that no chemical reaction occurred between the alloy melt and the denucleating glass. Accordingly, the alloy composition remains almost unchanged by undercooling (Table 1). However, the undercooling process gives rise to a pronounced change in the microstructure of  $\text{Co}_2\text{NiGa}$  alloys, as is illustrated in Fig. 3. By peritectic reaction, the  $\gamma$  phase forms as a coarse dendrite in casting (Fig. 3a) but as an equiaxed grain in undercooling (Fig. 3b–f). Similar to what was found in

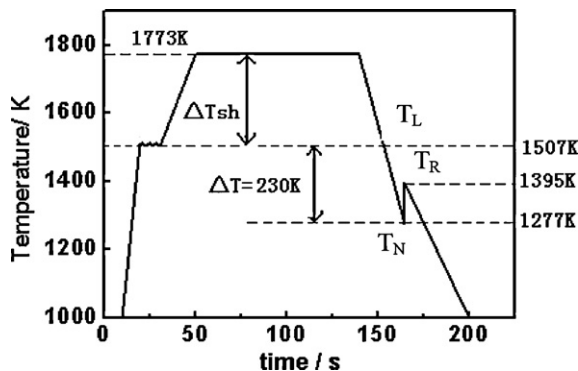


**Fig. 2.** Typical cooling curve of undercooled  $\text{Co}_2\text{NiGa}$  alloys melts with  $\Delta T = 230$  K.  $\Delta T_{sh}$ , superheating temperature;  $T_L$ , liquidus temperature;  $T_R$ , recalescence temperature;  $T_N$ , nucleation temperature.

**Table 1**

Chemical composition of  $\text{Co}_2\text{NiGa}$  alloys measured by EDX.

Alloy	Chemical composition (at.%) ( $\pm 0.5\%$ )		
	Co	Ni	Ga
As-cast	49.9	25.0	25.1
$\Delta T = 230$ K	50.0	25.2	24.8

undercooled  $\text{Ni}_{60}\text{Fe}_{17.5}\text{Ga}_{22.5}$  alloys by our previous work [14], as the degree of undercooling increases, the size of typical  $\gamma$  phase is substantially refined, the distribution of particles becomes relatively homogeneous, and the volume fraction of  $\gamma$  phase gradually increases (Fig. 4). When the volume fraction of  $\gamma$  phase increases by large undercooling, for the  $\beta$  phase, the Ga content increases while the Co and Ni contents decrease (Table 2).

The basic difference between equilibrium solidification and large undercooling solidification lies in the temperature gradient ( $G_L$ ) at the solid/liquid interface. For equilibrium solidification,  $G_L > 0$ , and the latent heat of primary solid phase is released by the solid, whereas for the high undercooling solidification,  $G_L < 0$ , the latent heat can be absorbed by both primary dendrites and undercooled melt [6,7]. The solidification process of undercooled  $\text{Co}_2\text{NiGa}$  alloy is as follows: initially, when the alloy is undercooled below its equilibrium liquidus temperature, high driving force for crystallization occurs, and any disturbance from the crystal surface would induce the nucleation abruptly [15] with the  $\gamma$  dendrites forming at the nucleation site and rapidly propagating through the melt. The abrupt release of fusion heat during the dendrite growth leads to rapid recalescence, and this is similar to the annealing processing of solidified crystals. Finally, peritectic reaction with solidification takes place between the residual interdendritic liquid and the  $\gamma$  phase at low melt undercooling in post-recalescence. Previous reports suggest that the solidification of undercooled melts is also initiated by heterogeneous surface nucleation. According to classical nucleation theory [16], the activation energy  $\Delta G^*$  for the formation of a critical nucleus is given by

$$\Delta G^* = \frac{16\pi\sigma^3}{3\Delta G_V^2} f(\theta) \quad (1)$$

where  $\sigma$  is the interfacial energy of the solid–liquid interface,  $f(\theta)$  the catalytic potency factor for heterogeneous nucleation, and  $\Delta G_V$  the Gibbs free energy difference for phase formation.  $\Delta G_V$  is calculated by [17]

$$\Delta G_V = \Delta S_f \Delta T - \frac{\Delta S_f}{\ln(T_L/T_0)} \left[ \Delta T - T \ln \left( \frac{T_L}{T} \right) \right] \quad (2)$$

where  $\Delta S_f$  is the entropy of fusion,  $T$  the system temperature, and  $T_L$  the liquidus temperature. The steady state nucleation rate,  $I$ , can be expressed as [16]

$$I = \frac{k_B T \xi N_A}{3\eta(T) a_0^3} \exp \left( - \frac{\Delta G^* f(\theta)}{k_B T} \right) \quad (3)$$

where  $k_B$  is the Boltzmann constant,  $\xi$  the potential nucleation sites fraction,  $N_A$  the Avogadro's number,  $a_0$  the interatomic distance, and  $\eta(T)$  the temperature-dependent viscosity of the undercooled

**Table 2**

Chemical composition of the  $\beta$  and  $\gamma$  phases in  $\text{Co}_2\text{NiGa}$  alloys.

Alloy		Chemical composition (at.%) ( $\pm 0.5\%$ )		
		Co	Ni	Ga
As-cast	$\beta$ phase	42.4	27.9	29.7
	$\gamma$ phase	56.3	22.7	21.0
$\Delta T = 230$ K	$\beta$ phase	41.8	27.4	30.8
	$\gamma$ phase	55.3	23.7	21.0

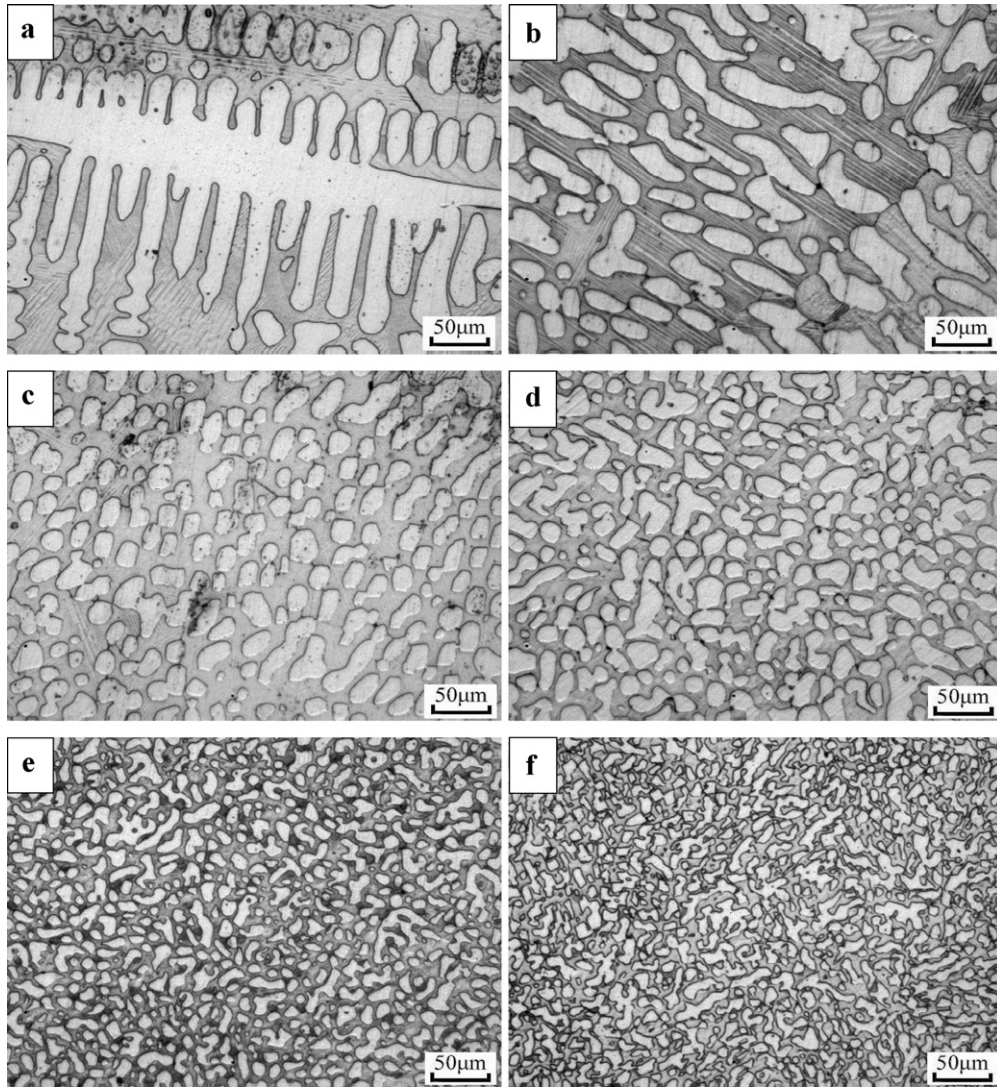


Fig. 3. Microstructure evolution of  $\text{Co}_2\text{NiGa}$  alloys with melt undercooling  $\Delta T=0$  K (a), 33 K (b), 77 K (c), 121 K (d), 190 K (e), and 230 K (f).

melt. The temperature-dependent viscosity can be approximated by the Vogel–Fulcher–Tammann equation

$$\eta(T) = \eta_0 \exp \left( \frac{A}{T - T_0} \right) \quad (4)$$

where  $\eta_0$  is the viscosity of alloy in melting temperature and  $T_0$  the ideal glass transition temperature ( $\approx 2/3T_m$ ).

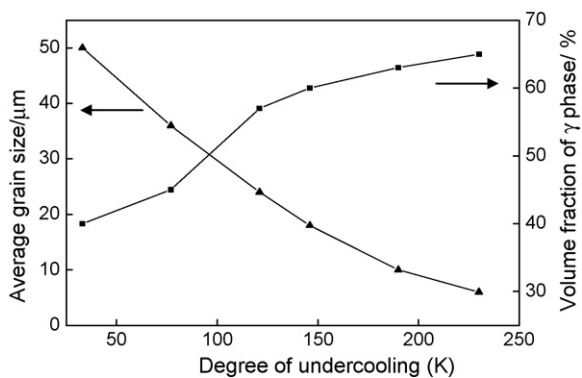


Fig. 4. Grain size and volume fraction of the  $\gamma$  phase as a function of the melt undercooling of  $\text{Co}_2\text{NiGa}$  alloys.

Based on Eqs. (1)–(4) above, the nucleation rate grows with increasing undercooling and causes decreasing size of the  $\gamma$  phase in  $\text{Co}_2\text{NiGa}$  alloys.

With increasing the degree of undercooling, the volume fraction of  $\gamma$  phase increases, which should affect the  $M_s$  of  $\text{Co}_2\text{NiGa}$

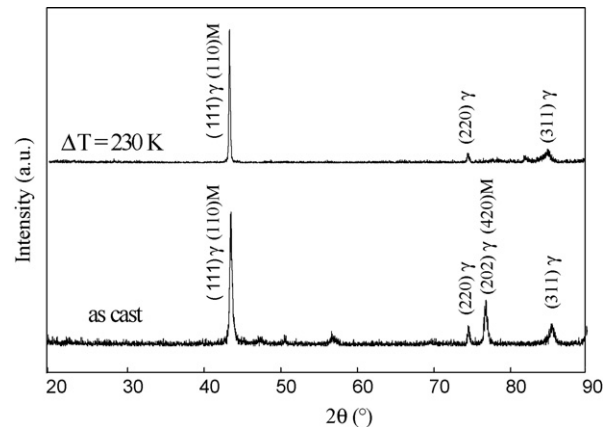


Fig. 5. XRD patterns of as-cast and undercooled  $\text{Co}_2\text{NiGa}$  alloys.

alloys. However, the martensitic transformation was not detected in undercooled Co<sub>2</sub>NiGa alloys (at least in the DSC measurement). The reason is probably due to the presence of the large amount of the  $\gamma$  phase in Co<sub>2</sub>NiGa alloys, which constrains the martensitic transformation of the matrix. This phenomenon was also observed in other MSM alloys, e.g. Ni–Fe–Ga–Co [18].

Fig. 5 shows the XRD patterns of as-cast and undercooled Co<sub>2</sub>NiGa alloys. Compared with the as-cast sample, the peak intensity of (1 1 1) $\gamma$  and (1 1 0) martensite (M) in the undercooled sample is much higher than that of the other peaks, and this indicates preferred orientation in (1 1 1) $\gamma$  and (1 1 0) M. In this sense, undercooled directional alloys with preferred orientation and excellent properties can be expected in the future by exciting the Co<sub>2</sub>NiGa melt at approximately 230 K undercooling.

#### 4. Conclusions

- (1) By using glass fluxing combined with superheating cycling method, the Co<sub>2</sub>NiGa magnetic shape memory alloy achieves 230 K maximum undercooling with no composition changed.
- (2) The grain size and the volume fraction of the  $\gamma$  phase in as-solidified Co<sub>2</sub>NiGa alloys can be controlled by melt undercooling. With the increasing of undercooling, the grain size decreases, their distribution becomes homogeneous, and their volume fraction grows. Meanwhile, the undercooled alloy shows an obvious preferred orientation.
- (3) The refinement of the  $\gamma$  phase in Co<sub>2</sub>NiGa alloys with melt undercooling can be explained within the framework of classical nucleation theory.

#### Acknowledgement

The authors are grateful to the financial support of the National Natural Science Foundation of China (Grant No. 50671068).

#### References

- [1] K. Oikawa, T. Ota, F. Gejima, T. Ohmori, R. Kainuma, K. Ishida, *Mater. Trans.* 42 (2001) 2472.
- [2] C. Craciunescu, Y. Kishi, T.A. Lograsso, M. Wutting, *Scr. Mater.* 47 (2002) 285.
- [3] Y.X. Li, H.Y. Liu, F.B. Meng, *Appl. Phys. Lett.* 84 (2004) 3594.
- [4] K. Prusik, B. Kostrubiec, T. Goryczka, G. Dercz, P. Ochcin, H. Morawie, *Mater. Sci. Eng. A* 481–482 (2008) 330.
- [5] D.L. Li, G.C. Yang, Y.H. Zhou, *Mater. Sci. Lett.* 11 (1992) 1033.
- [6] Z. Zhou, H. Fu, *J. Mater. Sci. Lett.* 19 (2000) 1491.
- [7] G. Song, M. Lee, W. Kim, D. Kim, Z. Zhang, X. Lin, G. Yang, Y. Zhou, *Mater. Trans. JIM* 41 (11) (2000) 1569.
- [8] F. Liu, X.F. Guo, G.C. Yang, *J. Cryst. Growth* 219 (2000) 489.
- [9] F. Liu, X.F. Guo, G.C. Yang, *Mater. Sci. Eng. A* 291 (2000) 190.
- [10] W.Z. Ma, H.X. Zheng, M.X. Xia, J.G. Li, *J. Alloys Compd.* 379 (2004) 188.
- [11] J.K. Zhou, J.G. Li, *J. Alloys Compd.* 461 (2008) 113.
- [12] J.K. Zhou, J.G. Li, *Appl. Phys. Lett.* 92 (2008) 141915.
- [13] J. Liu, Y.Q. Huo, H.X. Zheng, J.G. Li, *Mater. Lett.* 60 (2006) 1693.
- [14] H.X. Zheng, M.X. Xia, J. Liu, J.G. Li, *J. Alloys Compd.* 388 (2005) 172.
- [15] J.H. Perepezko, *Mater. Sci. Eng. A* 226–228 (1997) 374.
- [16] D. Turnbull, *Contemp. Phys.* 10 (1969) 473.
- [17] D.M. Herlach, F. Gillessen, T. Volkman, M. Wollgarten, K. Urban, *Phys. Rev. B* 46 (1992) 5203.
- [18] J. Liu, N. Scheerbaum, D. Hinz, O. Gutfleisch, *Scr. Mater.* 59 (2008) 1063.